Proceedings of the Twenty-second (2012) International Offshore and Polar Engineering Conference **www.isope.org**
Rhodes, Greece, June 17–22, 2012

ISBN 978-1-880653-94–4 (Set); ISSN 1098-6189 (Set)

Buried Steel Pipelines Crossing Strike-Slip Faults

Polynikis Vazouras[1], Spyros A. Karamanos[2], Panos Dakoulas[1]

[1] Department of Civil Engineering
University of Thessaly, Volos, Greece

[2] Department of Mechanical Engineering
University of Thessaly, Volos, Greece

ABSTRACT

The paper examines the behaviour of buried steel pipelines crossing active strike-slip faults. The vertical fault plane is crossed by the pipeline at an angle ranging between zero and 45 degrees, causing significant plastic deformation in the pipeline. The investigation is numerical, simulating the nonlinear response of the soil-pipeline system rigorously through nonlinear finite elements, accounting for inelastic material behaviour of the pipeline and the pipe and the soil, as well as contact and friction on the soil-pipe interface. Steel pipes with D/t ratio and material grade typical for hydrocarbon pipelines are analyzed, through an incremental application of fault displacement and appropriate pipeline performance criteria, defined within a strain-based design framework, are monitored throughout the analysis. The effects of various soil and linepipe parameters on the structural response of the pipeline are examined. The numerical results from the present investigation determine the fault displacement at which the specified performance criteria are reached, including the effects of internal pressure.

KEY WORDS: Pipeline; buckling; seismic fault; finite elements; strain-based design; performance criteria; soil-structure interaction.

INTRODUCTION

Ground-induced actions due fault movements are responsible for significant damages in oil and gas buried steel pipelines. Those deformations are applied in a quasi-static manner, and are not necessarily associated with high seismic intensity, but the pipeline may be seriously deformed, well beyond the elastic range of pipe material and may cause pipeline failure; high tensile stresses may cause fracture of the pipeline wall, especially at welds or defected locations or welds, whereas compressive stresses may cause buckling, in the form of pipe wall wrinkling, also referred to as "local buckling" or "kinking".

The pioneering work of Newmark and Hall (1975) has been extended by Kennedy et al. (1977), Wang and Yeh (1985), Wang and Wang (1995)and Takada et al. (2001) through a beam-type approach for describing pipeline deformation. More recent works on this subject have been reported by Karamitros et al. (2007) Liu et al. (2008)and Trifonov & Cherniy (2010). In addition to the above analytical and numerical studies, notable experimental works on the effects of strike-slip faults on buried high-density polyethylene (HDPE) pipelines have been reported in series of recent papers by Ha et al. (2008) and Abdoun et al. (2009).

The analytical works outlined above have modelled soil conditions based on a spring-type approach. A more rigorous approach has been followed in a most recent paper (Vazouras, Karamanos, Dakoulas, 2010) of the present authors, for buried steel pipelines crossing strike-slip faults at right angle with respect to the fault plane, through a finite element modelling of the soil-pipeline system, which accounts rigorously for the inelastic behaviour of the surrounding soil, the interaction and the contact between the soil and the pipe (including friction contact and the development of gap), the development of large inelastic strains in the steel pipeline, the distortion of the pipeline cross-section and the possibility of local buckling, the presence of internal pressure.

The present paper extends the work presented by Vazouras et al. (2010), considering buried steel pipelines crossing the vertical fault plane at various angles. Furthermore, the paper examines the mechanical behaviour of buried steel pipelines with respect to appropriate performance criteria, expressed in terms of local strain or cross sectional deformation. The fault displacements corresponding to those performance criteria are identified, in the framework of a performance-based pipeline design. Pipes from two steel grades (X65 and X80), widely used in buried pipeline applications, are considered for typical values of diameter-to-thickness ratio D/t (ranging from 72 to 144). The performance of pressurized pipes with respect to non pressurized pipes is also examined in terms of each performance criterion. Numerical results are presented in the form of diagrams, depicting the fault displacement corresponding to a specific performance criteria with respect to the crossing angle.

PERFORMANCE CRITERIA FOR STRAIN-BASED DESIGN OF BURIED STEEL PIPELINES

Under strong permanent ground-induced actions, buried steel pipelines exhibit severe deformation beyond the elastic limit. Steel material is quite ductile and capable of sustaining significant amount of

inelastic deformation, but at locations where large tensile strains develop, rupture of the pipeline wall may occur. Wrinkling (local buckling) of pipeline wall may also occur due to excessive compression at the pipeline wall, followed by pipe wall folding and development of significant local strains. Furthermore, severe distortions of the pipeline cross-section may render the pipeline non-operational. To quantify the amount of damage in a buried pipeline under severe ground-induced action, the following three performance criteria are monitored in the present analysis: (a) tensile strain equal to 3% and 5% in the longitudinal direction of the pipeline, which may cause pipe wall rupture, (b) local buckling (wrinkling) formation, and (c) excessive distortion of the pipeline cross-section so that the "flattening parameter" f defined $f = \Delta D/D$ (ΔD is the change of pipe diameter in the flattening direction) reaches a value of 0.15. During the consecutive stages of fault displacement application, the performance criteria are evaluated, monitoring the maximum values of longitudinal strain along the pipeline, as well as the cross-sectional distortion (flattening) at various cross-sections. Furthermore, the finite element model is capable of simulating rigorously the formation of pipeline wall wrinkling.

NUMERICAL MODELING

The mechanical response of steel pipelines under strike-slip fault movement is examined numerically, using general-purpose finite element program ABAQUS. The model is an enhancement of the one presented by Vazouras et al. (2010). The pipeline is embedded in an elongated soil prism along the x axis shown in Figure 1a. Figure 1b shows the soil mesh in the y-z plane and Figure 1c depicts the mesh for the steel pipe. Four-node reduced-integration shell elements (type S4R) are employed for modeling the cylindrical pipeline segment, and eight-node reduced-integration "brick" elements (C3D8R) are used to simulate the surrounding soil. The top surface of the prism represents the soil surface, and the burial depth is chosen equal to about 2 pipe diameters, which is in accordance with pipeline engineering practice (Gresnigt,1986). The prism length in the x direction is equal to at least 65 pipe diameters, whereas dimensions in directions y, z equal to 11 and 5 times the pipe diameter respectively .

The central part of the pipeline around the fault has a fine mesh of elements. A total of 54 shell elements around the pipe circumference in this central are used, whereas the size of the shell elements in the longitudinal direction has been chosen equal to 1/26 of the pipeline outer diameter D. The fault plane divides the soil in two blocks of equal size (Figure 1a) and the finite element mesh for the soil is more refined in the region near the fault.

The analysis is conducted in two steps as follows; gravity loading is applied first and, in the second step, fault movement is imposed, using a displacement-controlled scheme, which increases gradually the fault displacement d. The vertical boundary nodes of the first block remain fixed in the horizontal direction, whereas a uniform displacement due to fault movement is imposed in the external nodes of the second (moving) block along the horizontal n direction, which is parallel to the fault plane. For the case of pressurized pipelines an intermediate step of internal pressure application is considered (after the application of gravity and before the fault displacement is activated).

The angle β between the fault direction n and always the y direction is a main parameter of the present study (Figure 1). Positive values of β indicate that the fault movement induces tension to the pipeline, whereas negative values of β refer to fault movements that result in pipeline compression. The fault movement is considered to occur within a narrow transverse zone of width w, equal to 0.33m.

The steel pipe material is described with a large-strain von Mises plasticity model with isotropic hardening, and its calibration is performed through an appropriate uniaxial stress-strain curve from a tensile test on a coupon specimen. The mechanical behavior of soil material is described through an elastic-perfectly plastic Mohr-Coulomb constitutive model, characterized by the soil cohesiveness c, the friction angle ϕ, the elastic modulus E, and Poisson's ratio ν. The dilation angle ψ is assumed equal to zero for all cases considered in this paper.

The soil-pipe interface is simulated with a contact algorithm, which allows separation of the pipe and the surrounding soil, and accounts for interface friction, through an appropriate friction coefficient μ, equal to 0.3.

NUMERICAL RESULTS

Numerical results are obtained for X65 and X80 steel pipelines for typical values of the diameter-to-thickness ratio, and for different soil conditions (cohesive soils). The outer diameter D of the pipe is equal to 914.4 mm (36 in), which is a typical size for oil and gas transmission pipelines. Four values for the pipe wall thickness are considered, namely 6.35 mm (¼ in) 9.53 mm (⅜ in), 12.7 mm (½ in) and 15.88 mm (⅝ in), corresponding to D/t values equal to 144, 96, 72 and 57.6 respectively, which cover a wide range of oil and gas pipeline applications. Note that the first value corresponds to relatively thin-walled pipes ($D/t = 144$), which may also be used for water transmission pipelines.

The seismic fault plane passes through the middle cross-section of the pipeline and crosses the pipeline axis at different angles, so that the value of angle β ranges between -10 degrees and 45 degrees (the minus sign indicates a configuration where the pipeline is subjected to global compression as shown in Figure 1).

Non-Pressurized X65 Steel Pipelines

Buried X65 steel 36-inch-diameter pipelines are examined first, in the absence of internal pressure, considering cohesive soil conditions, with appropriate values of soil parameters c, φ and E. The API 5L X65 steel material is a typical steel material for oil and gas pipeline applications, with a nominal stress-engineering strain curve shown with dashed line in Figure 2, obtained from a uniaxial tensile test. The yield stress σ_y is equal to 448.5 MPa (65 ksi) followed by a plastic plateau up to 1.48% strain and, subsequently, by a strain-hardening regime with a hardening modulus equal to about $E_s/300$, where E_s is the Young's modulus of the steel material, equal to 210 GPa. Considering a safety (reduction) factor equal to 0.72, as suggested in American Society of Mechanical Engineers (2007) and Comité Européen de Normalisation (2006), the maximum operating pressure $p_{\max}$ of this pipeline, given by the following expression

$$p_{\max} = 0.72 \times \left(2\sigma_y \frac{t}{D} \right) \quad (1).$$

A buried steel pipeline with wall thickness equal to ⅜-inch, embedded in a soft-to-firm clay soil is considered first. This clay is referred to as Clay I and, under "undrained" loading conditions, it has a cohesion c = 50 kPa, friction angle $\varphi = 0^{\circ}$, Young's modulus E = 25 MPa and Poisson's ratio ν = 0.3. Figure 3a depicts the shape of the deformed pipeline at fault displacements d = 0.4 m, 1.37 m, 2 m and 2.9 m in the area near the fault, crossing the fault at a right angle, i.e.

the β angle is equal to zero degrees. Moreover, Figure 3b depicts the shape of the deformed pipeline and the distribution of the longitudinal normal strain ε_x on its outer surface at the same four values of fault displacement. At a value of fault displacement equal to $d = 0.43$ m, the pipeline wall exhibits local buckling, in the form of a short-wave wrinkling pattern. It should be noted that the wrinkling pattern is formed gradually with increasing fault displacement, so that a criterion for identifying the onset of local buckling is necessary. In the present study, the onset of buckling is defined as the stage where outward displacement of the pipe wall starts at the area of maximum compression, a criterion also adopted in Vazouras-Karamanos and Dakoulas, (2010), and the corresponding fault displacement is referred to as "critical fault displacement" (d_{cr}).

At that stage, bending strains due to pipe wall wrinkling develop, associated with significant tensile strains at the "ridge" or "crest" of the buckle, so that the longitudinal compressive strains at this location at the outer surface of the pipe wall start decreasing, forming a short wavy pattern at this location. At the onset of local buckling, the longitudinal compressive strain at the buckle location (ε_{cr}) is equal to 6.897×10^{-3}, whereas the maximum tensile strain ($\varepsilon_{T,\max}$) on the opposite side of the pipe is 3.54×10^{-3}, which is substantially less lower than the strain that would cause tensile failure in the form of rupture in a non-seriously-defected pipeline. Under increasing fault displacement, the wrinkled pattern further develops, resulting in a significant localization of deformation at the buckled area. However, this wrinkle development occurs up to a fault displacement equal to 1.37m, whereas beyond this value, the depth of the buckle (i.e. the wrinkling wave amplitude) starts decreasing due to longitudinal stretching of the pipeline, as shown in Figure 3b for values of fault displacements d equal to 1.37 m and 2.9 m. Furthermore, as the total pipeline length increases with continued fault movement due to longitudinal stretching, it results to higher tensile strains in the longitudinal direction, whereas the corresponding compressive strains become smaller. This is shown in Figure 3b where for a fault displacement of d = 2.9 m, compressive longitudinal strains are significantly lower than those corresponding to a fault displacement of d = 1.4 m.

Beyond the formation of the local buckle, and for fault displacement greater than 1.50m, significant distortion of the cross-section in terms of ovalization is observed. The cross-section with maximum distortion of pipeline cross-section is located at a distance of 0.5 m from the fault, and the corresponding flattening parameter reaches the critical value of 0.15 at a fault displacement equal to $d = 1.71$ m. In addition, the maximum tensile longitudinal strain of the pipe is significantly increased, on either side of the pipeline cross-section, which may lead to local fracture at welds or other locations where minor defects exist. For a fault displacement of d = 1.62 m the maximum tensile strain is equal to 3%, a critical value as it discussed above. At the end of the analysis (fault displacement equal to 4m), the longitudinal tensile strain limit of 5% has not been reached at any location of the pipeline wall.

The X65 36-inch-diameter $\frac{3}{8}$-inch-thick pipeline, embedded in the same soft-to-firm clay soil conditions (Clay I), is also examined for various crossing angles. Figure 4 shows the deformed shapes of the pipeline for a value of β equal to 25 degrees, at various fault displacements. At this angle, local buckling of the pipeline wall does not occur. The deformed shape shows a significant distortion of the pipeline cross-section in the form of ovalization. The amount of ovalization, measured according to the flattening parameter f reaches a critical value of 0.15 at fault displacement of 0.77 m, at the area where the pipe intersects with the fault. Under increasing fault movement, this ovalization pattern is further developed resulting in a severe distortion of the pipe cross-section, associated with negative hoop curvature of the pipeline wall, sometimes referred to as "inversion", for a fault displacement of d = 1.45 m, as shown in Figure 4. The critical longitudinal tensile strain limits of 3% and 5% appear at a fault displacements d = 0.58 m and d = 1.15 m respectively, one meter away from fault.

The response becomes quite different if a crossing angle β of opposite (negative) sign is considered. In this case, the fault motion is associated with a decrease of length of the pipeline, resulting in the development of significant compressive stresses and strains, leading to local buckling. In Figure 5, the performance of the above X65 $\frac{3}{8}$-inch-thick steel pipeline is shown for Clay I soil conditions, crossing the fault plane at an angle of β equal to -10 degrees. The critical fault displacement where wrinkling initiates has been computed equal to 0.225 m at a cross- section 3.6 meters away from fault. At this point the values of compressive strain at buckle is -5.32×10^{-3}, whereas the corresponding maximum tensile strain on the opposite side of the pipeline wall is equal to 1.01×10^{-3}. Upon continuation of fault displacement, the buckle pattern is further developed resulting in folding of the pipeline wall and inversion of the buckled pipeline cross-section at fault displacement d=0.75 m. Tension strain of 3% occurs at fault displacement d=0.49 m and 5% at d=0.67 m. Ovalization is reached at d=2.30 m, at a distance of 0.50 m from the fault.

The above numerical results for the X65 are shown in graphical form in Figure 6, where the fault displacement values corresponding to the performance criteria, namely (a) local buckling, (b) longitudinal strain equal to 3%, (c) longitudinal strain equal to 5% and (d) cross-sectional flattening $f = 0.15$, are plotted with respect to the crossing angle β. The results indicate that for non-positive values of angle β, local buckling is the dominant limit state. For positive values of angle β two major limit states, namely the 3% longitudinal tensile strain and the cross section flattening are most important. For values of β up to about 15 degrees, cross sectional flattening is reached first whereas for greater values of β the 3% tensile strain criterion becomes the dominant limit state. It is further observed that an increase of the value of β results in a significant decrease of the value of critical fault displacement.

In Figure 7, Figure 8 and Figure 9 the fault displacement values corresponding to the three performance criteria are plotted with respect to the crossing angle β for X65 pipelines with D/t ratios equal to 144, 72 and 57.6 respectively. The results indicate that the behavior has several similarities with the results in Figure 6. Nevertheless, the results show a significant dependence of the critical fault displacement with respect to the D/t ratio. Local buckling is observed at non-positive values of β. In addition, for the thin-walled pipeline (D/t = 144) local buckling may also occur for small positive values of β ($\beta = 5^o$) at a value of fault displacement equal to 0.52 m. With increasing fault displacement, the local buckle does not develop further and its size is reduced due to longitudinal stretching. For all cases with positive values of β, the flattening limit state and the 3% tensile strain limit state are dominant, similar to the case of D/t = 96. The angle β at which the 3% tensile strain limit state becomes critical over the flattening limit state depends on the D/t ratio.

The response of the above X65 steel pipeline (D/t = 96), buried in stiffer cohesive soil conditions, is examined, assuming values of soil

parameters c, E and φ are equal to 200 kPa, 100 MPa and 0°, respectively. They correspond to a stiff clay under "undrained conditions", referred to as Clay II. The numerical results indicate that the bending deformation of the pipeline in stiff soil occurs within a short distance from the fault location. For the particular case of $\beta = 0$, the critical cross-section is at a distance of 2.5 m from the fault. The results are shown in Figure 10 and their comparison with the results shown in Figure 6 for Clay I soil conditions demonstrates the significant effect of site conditions on the response of the steel pipeline; in the case of a stiff soil bending deformation affects a smaller length of the pipeline so that higher bending stresses and strains develop for the same fault displacement d, than those in the case of a soft soil, and the performance limits for the stiff soil are reached at significantly lower value of fault displacement. Furthermore, in stiff soil conditions,. Figure 11 depict the corresponding results for X65 pipelines with D/t equal to 144. The results, compared with Figure 6, Figure 7 indicate a significantly lower deformation capacity for those stiff soil conditions. Furthermore, the results show that for positive values of angle β the 3% tensile strain is the governing mode of failure. Depending on pipeline thickness, local buckling may also occur at positive values of angle β. More specifically, local buckling occurs for $\beta = 5^o$ in the case of D/t equal to 72 and 96, whereas for the case of thin-walled pipeline ($D/t = 144$) local buckling occurs even at $\beta = 10^o$.

Effects of Internal Pressure

The effects of internal pressure on pipeline mechanical behavior are investigated considering internally pressurized X65 pipelines with thickness of $^3/_8$ inch, embedded in soft-to-firm soil conditions (Clay I). The numerical results presented in Figure 12 and Figure 13 correspond to a pressure level of 38 barr, which is equal to 56% of the maximum operating pressure $p_{\max}$ expressed by equation (1), whereas the results in Figure 14 and Figure 15 show the corresponding results for a lower pressure level equal to 26 barr, which is 38% of $p_{\max}$. At those levels of internal pressure, cross sectional distortion of the pipeline is quite small and flattening does not reach the critical value of 0.15. For non-positive values of angle β buckling occurs. The buckled shapes of the pressurized pipelines are shown in Figure 16 and are quite different from the buckled shapes of the non-pressurized pipelines shown in in the same figure. Nevertheless, the corresponding values of critical fault displacement d_{cr} (0.41 m for 38% of $p_{\max}$ and 0.39 m for 56% of $p_{\max}$) are somewhat lower than the corresponding value without pressure. This is attributed to the development of additional stresses and strains in the pipeline wall that cause early yielding and lead to a premature local buckling formation, an observation also noted in Vazouras-Karamanos and Dakoulas, (2010). The compressive strain along the critical generator of the steel pressurized pipeline at the onset of buckling is -8.5×10^{-3} and -7.2×10^{-3} for 56% and 38% of $p_{\max}$ respectively. For positive values of angle β, the 3% tensile strain criterion is the governing limit state.

Mechanical Behavior of X80 Steel Pipelines

The behavior of buried high-strength steel X80 pipelines under fault-induced deformation is also analyzed, using the numerical tools described in the previous sections. The nominal uniaxial tensile stress–strain relationship of the API 5L X80 material is plotted in Figure 2 with the solid material curve. The material has a yield stress of 596 MPa without a plastic plateau, corresponding to a cold expanded (UOE) line pipe. The maximum operating pressure $p_{\max}$ is given by equation (1).

Numerical results are obtained for 36-inch-diameter X80 steel pipelines with thickness equal to $^3/_8$-inch and ½-inch, corresponding to D/t values equal to 96 and 72 respectively, embedded in soft-to-firm cohesive soils (Clay I). The numerical results for zero pressure are summarized in Figure 17 and Figure 18, and indicate similar trends with those observed and discussed in the above paragraphs for the X65 pipelines. In both cases, local buckling of pipeline wall occurs at non-positive values of β. A comparison of these results with those in Figure 6 and Figure 7 for the X65 pipelines, indicate that buckling occurs at higher values of fault displacements. Nevertheless, for the specific case where $\beta = 0$ and D/t = 72, local buckling does not occur; in this case the compressive buckling strain is rather high due to high grade of steel and because of the tensile strains induced by longitudinal stretching, this critical strain is not reached. For positive values of angle β the ovalization performance criterion is reached first, for both value of D/t, up to an angle of β equal to about 40 degrees.

The behavior of pressurized X80 steel pipelines is shown in Figure 19 and Figure 20. For non-positive values of β, local buckling occurs and the corresponding values of critical fault displacement are similar, yet somewhat lower, than those of the non-pressurized X80 pipelines with the same D/t ratio. In addition, for positive values of angle β, cross-sectional shape of the pipeline remains quasi-circular, the flattening criterion is never reached, and the 3% longitudinal tensile strain is the governing limit state.

CONCLUSIONS

Using advanced finite element simulation tools, the mechanical behaviour of buried steel pipelines crossing active strike-slip faults was investigated. The pipeline is assumed horizontal crossing the fault plane at various angles. The main target is the investigation of the effects of the crossing angle for several soil and pipe parameters. The response under various cohesive conditions (expressed through various values of soil cohesion, friction and stiffness parameters (c, φ, E) on the structural response of the pipe are examined, with respect to three pipeline performance limits (a) maximum tensile strain, (b) local buckling and (c) cross-section flattening.

Numerical results are obtained for various values of D/t ratio and for X65 and X80 steel pipelines, which are representative for oil and gas applications. In the majority of the cases analyzed, it is shown that local buckling is the governing mode of failure for non-positive values of the crossing angle β. For pipelines under tension (positive values of β) local buckling is not dominant; in those pipelines, the governing modes of failure are the 3% value of longitudinal tensile strain and the cross-sectional flattening. Nevertheless, buckling may also occur for small positive values of β, if the pipeline is thin-walled and the ground conditions are quite stiff.

The numerical results are presented in diagram form for normalized ultimate fault displacement in terms of the crossing angle, and indicate a strong dependence in terms of the pipeline diameter-to-thickness ratio D/t. It is concluded that in softer ground conditions result in a larger deformation capacity of the pipeline. Furthermore, the presence of internal pressure prevents cross-sectional distortion, and induces additional stresses, so that the deformation capacity of the pressurized

pipeline is somewhat reduced compared with non-pressurized pipelines. The results also demonstrate the superior behaviour of high-strength X80 steel pipelines with respect to the behaviour of X65 pipelines.

REFERENCES

Abdoun T. H., Ha, D., O'Rourke, M. J., Symans, M. D., O'Rourke, T. D., Palmer, M. C., and Stewart, H. E. (2009), "Factors influencing the behavior of buried pipelines subjected to earthquake faulting.", *Soil Dynamics and Earthquake Engineering*, Vol. 29, pp. 415– 427.

American Society of Mechanical Engineers (2007), *Gas Transmission and Distribution Piping Systems*, ANSI/ASME B31.8.

Comité Européen de Normalisation (2006), *Eurocode 8, Part 4: Silos, tanks and pipelines*, CEN EN 1998-4, Brussels, Belgium.

Newmark N. M., Hall W. J. (1975), "Pipeline design to resist large fault displacement". *Proceedings of U.S. National Conference on Earthquake Engineering*; 416–425.

Gresnigt, A. M., (1986). "Plastic Design of Buried Steel Pipes in Settlement Areas", *HERON*, Vol. 31, (4), pp. 1-113.

Ha, D., Abdoun T. H., O'Rourke, M. J., Symans, M. D., O'Rourke, T. D., Palmer, M. C., and Stewart, H. E. (2008), "Buried high-density polyethylene pipelines subjected to normal and strike-slip faulting – a centrifuge investigation.", *Canadian Geotechnical Journal*, Vol. 45, pp. 1733-1742.

Ha, D., Abdoun T. H., O'Rourke, M. J., Symans, M. D., O'Rourke, T. D., Palmer, M. C., and Stewart, H. E. (2008), "Centrifuge Modelling of Earthquake Effects on Buried High-Density Polyethylene (HDPE) Pipelines Crossing Fault Zones.", *ASCE Journal of Geotechnical and Geoenvironmental Engineering*, Vol. 134, No. 10, pp. 1501-1515.

Karamitros, D. K., Bouckovalas, G. D., and Kouretzis, G. P. (2007), "Stress Analysis of Buried Steel Pipelines at Strike-Slip Fault Crossings.", *Soil Dynamics & Earthquake Engineering*, Vol. 27, pp. 200-211

Kennedy, R. P., Chow, A. W. and Williamson, R. A. (1977), "Fault movement effects on buried oil pipeline", *ASCE Journal of Transportation Engineering*, Vol. 103, pp. 617-633.

Liu, M., Wang, Y.-Y., and Yu, Z., (2008), "Response of pipelines under fault crossing.", *Proceedings, International Offshore and Polar Engineering Conference*, Vancouver, BC, Canada.

Takada, S., Hassani, N. and Fukuda, K. (2001), "A new proposal for simplified design of buried steel pipes crossing active faults", *Earthquake Engineering and Structural Dynamics*, 2001; Vol. 30: pp.1243–1257.

Trifonov, O. V. and Cherniy, V. P. (2010), "A semi-analytical approach to a nonlinear stress–strain analysis of buried steel pipelines crossing active faults.", *Soil Dynamics & Earthquake Engineering*, Vol. 30, pp. 1298-1308.

Vazouras, P., Karamanos, S. A., and Dakoulas, P. (2010), "Finite Element Analysis of Buried Steel Pipelines Under Strike-Slip Fault Displacements", *Soil Dynamics and Earthquake Engineering*, Vol. 30, No. 11, pp. 1361–1376.

Wang L. L. R., Wang L. J. (1995), Parametric study of buried pipelines due to large fault movement. *ASCE*, *TCLEE* 1995; (6):152–159.

Wang, L. R. L. and Yeh, Y. A. (1985), "A refined seismic analysis and design of buried pipeline for fault movement", *Earthquake Engineering & Structural Dynamics*, Vol. 13, pp. 75-96.

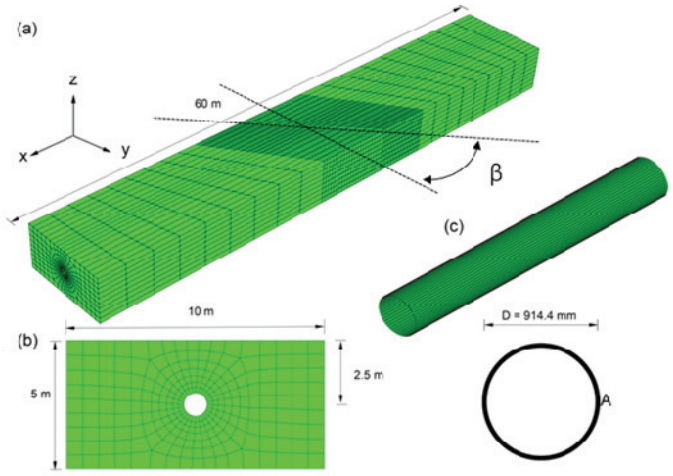

Figure 1: Finite element model of the (a) soil prism with tectonic strike-slip fault, (b) finite element mesh of soil prism cross-section and (c) finite element mesh of steel pipeline.

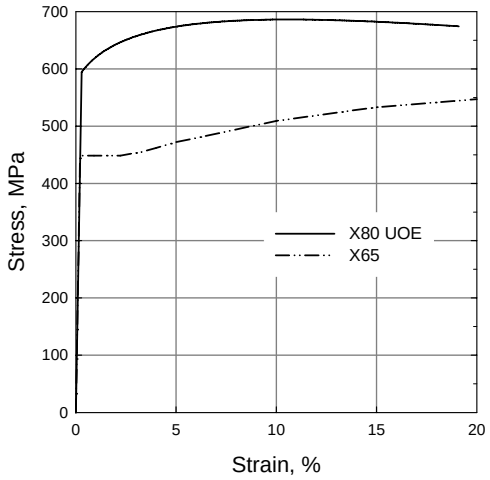

Figure 2: Uniaxial nominal stress-engineering strain curve for API 5L X65 steel and X80 steel.

(b)

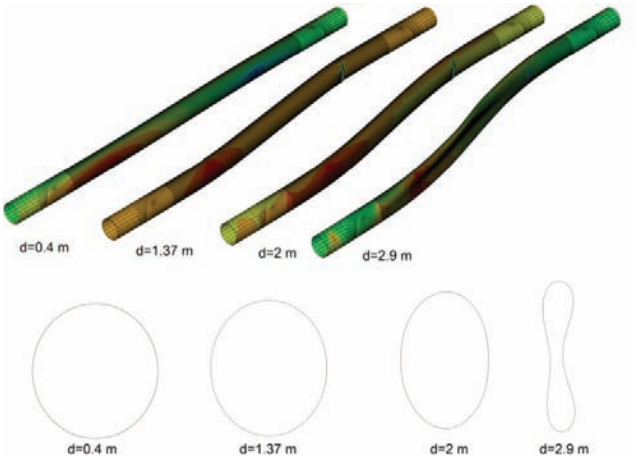

Figure 3: (a) plan view of deformed shape of a pipeline for d=1-4m and (b) distribution of longitudinal normal strain for seismic fault displacement equal to 0.4, 1.37, 2, 2.9m. The cross-sectional shapes refer to a location at 0.5 meters away from the fault.

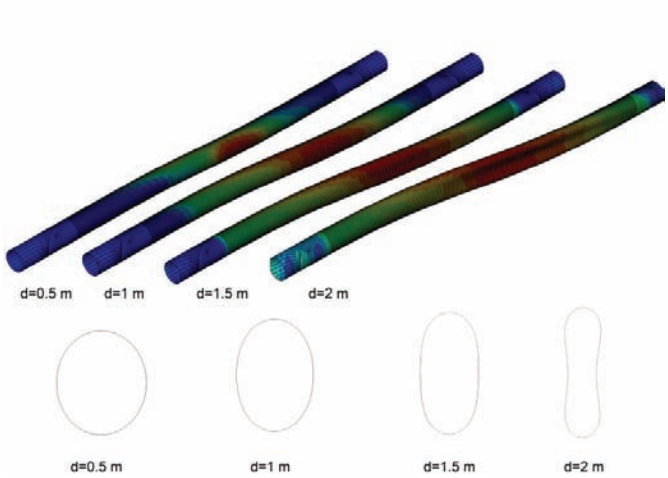

Figure 4: Deformed shape of the pipeline for a value of β equal to 25 degrees, at various fault displacements. The cross-sectional shapes refer to a location at 0.5 meters away from the fault.

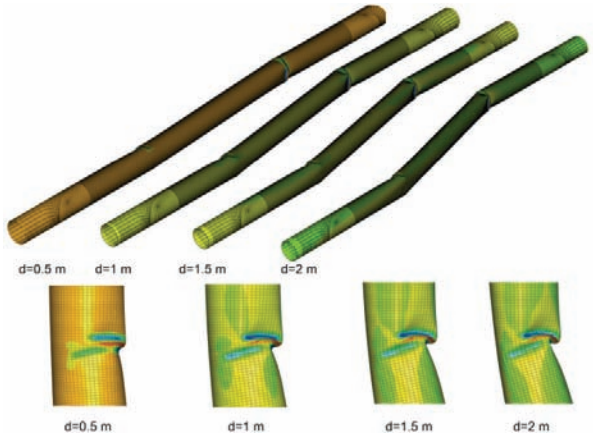

Figure 5: Deformed shape of the pipeline for a value of β equal to -10 degrees, at various fault displacements

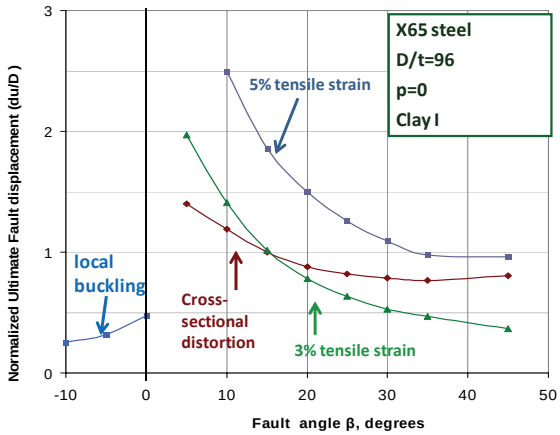

Figure 6: Normalized ultimate fault displacement for various performance limits at different angles of β (X65 pipe, Clay I, D/t=96, zero pressure).

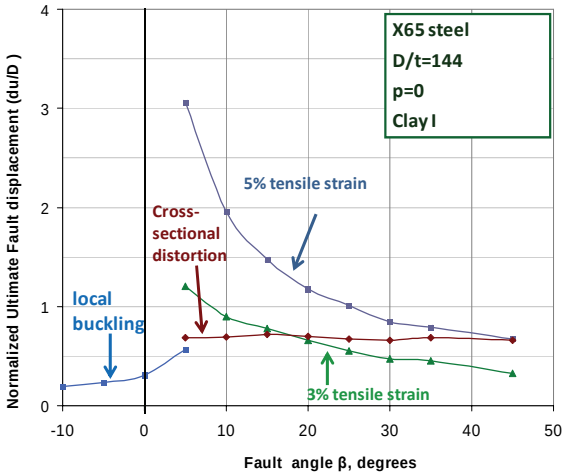

Figure 7: Normalized ultimate fault displacement for various performance limits at different angles of β (X65 pipe, Clay I, D/t=144, zero pressure)

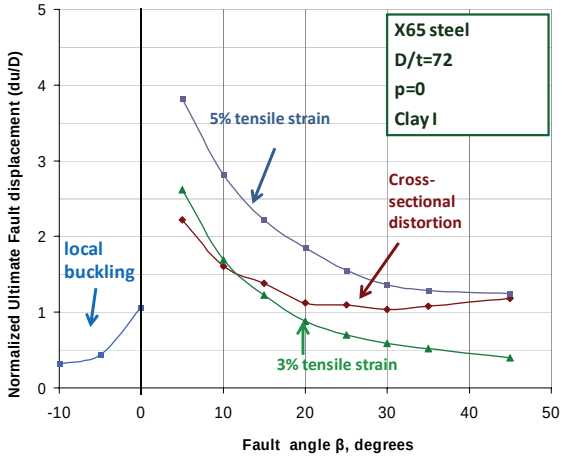

Figure 8: Normalized ultimate fault displacement for various performance limits at different angles of β (X65 pipe, Clay I, D/t=72, zero pressure)

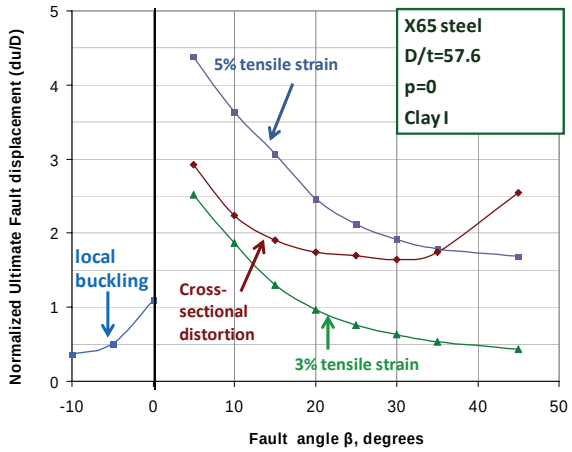

Figure 9: Normalized ultimate fault displacement for various performance limits at different angles of β (X65 pipe, Clay I, D/t=57.6, zero pressure)

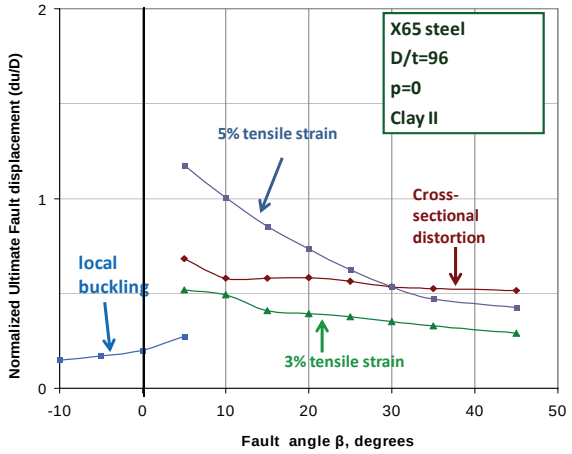

Figure 10: Normalized ultimate fault displacement for various performance limits at different angles of β (X65 pipe, Clay II, D/t=96, zero pressure)

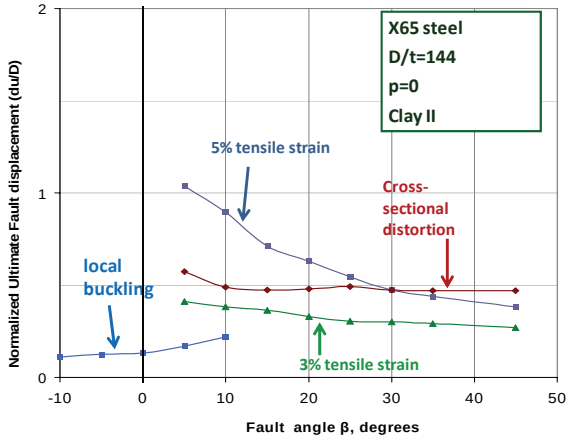

Figure 11: Normalized ultimate fault displacement for various performance limits at different angles of β (X65 pipe, Clay II, D/t=144, zero pressure)

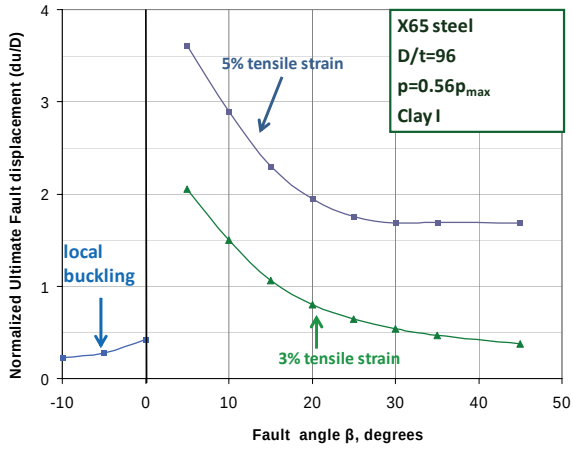

Figure 12. Normalized ultimate fault displacement for various performance limits at different angles of β (X65 pipe, Clay I, D/t=96, pressure 56% of p_{max})

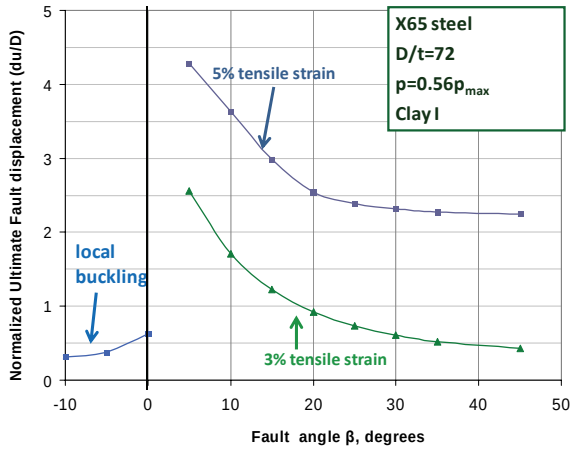

Figure 13. Normalized ultimate fault displacement for various performance limits at different angles of β (X65 pipe, Clay I, D/t=72, pressure 56% of p_{max})

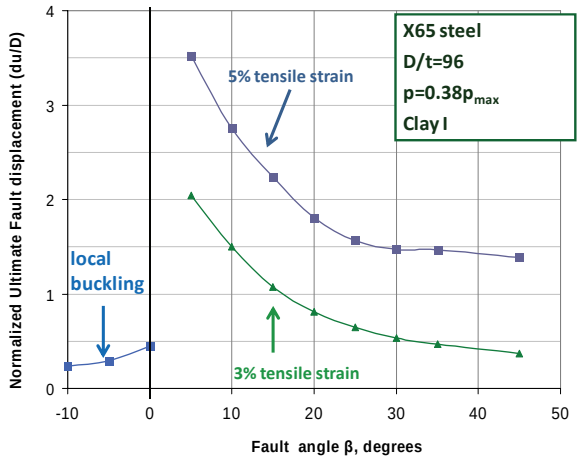

Figure 14: Normalized ultimate fault displacement for various performance limits at different angles of β (X65 pipe, Clay I, D/t=96, pressure 38% of p_{max})

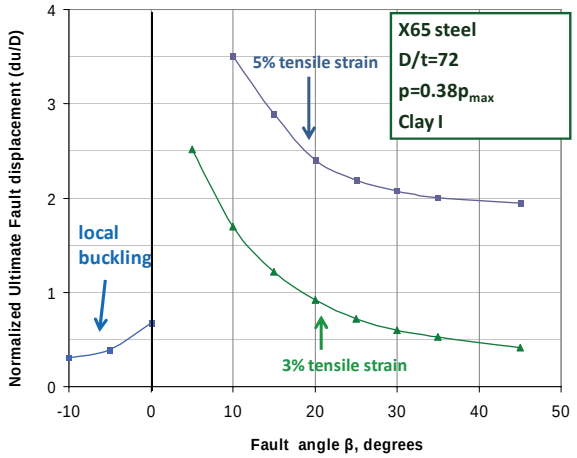

Figure 15: Normalized ultimate fault displacement for various performance limits at different angles of β (X65 pipe, Clay I, D/t=72, pressure 38% of p_{max})

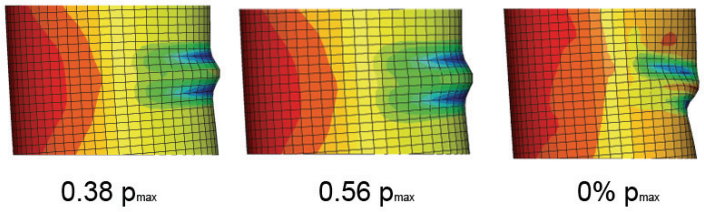

Figure 16: Comparison of buckled shapes between pressurized and non-pressurized pipes

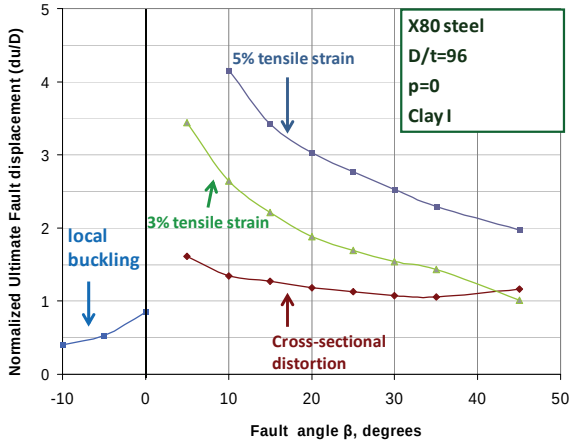

Figure 17: Normalized ultimate fault displacement for various performance limits at different angles of β (X80 pipe, Clay I, D/t=96, zero pressure)

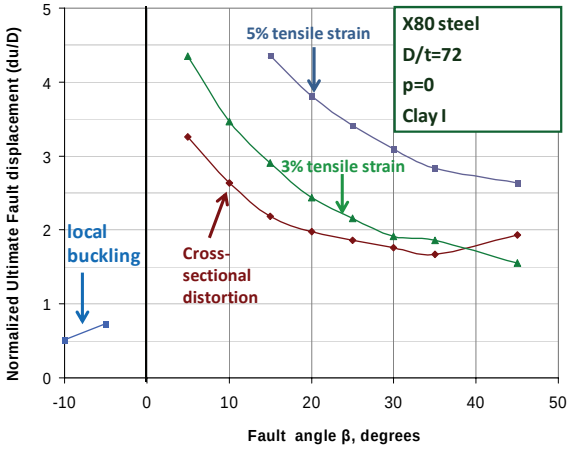

Figure 18: Normalized ultimate fault displacement for various performance limits at different angles of β (X80 pipe, Clay I, D/t=72, zero pressure)

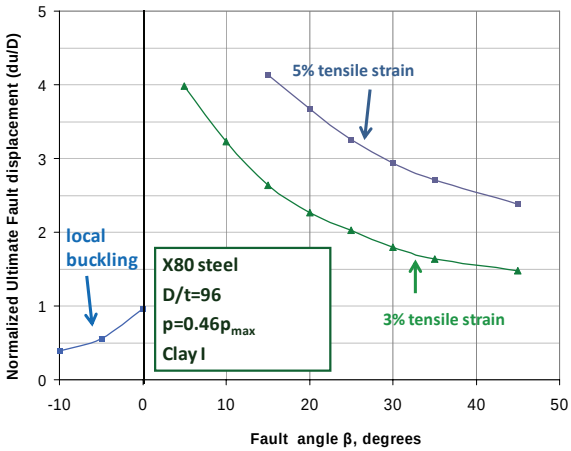

Figure 19: Normalized ultimate fault displacement for various performance limits at different angles of β (X80 pipe, Clay I, D/t=96, pressure 46% of p_{max})

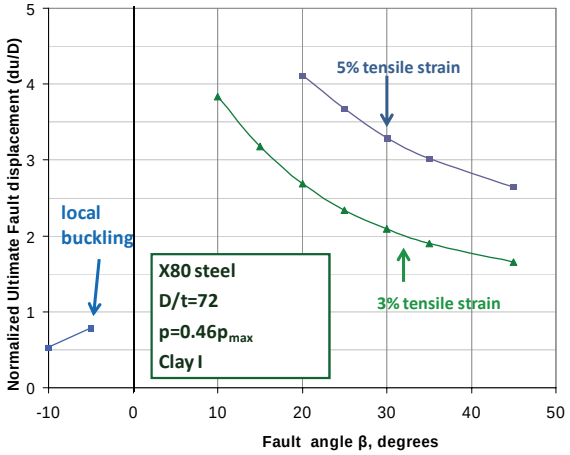

Figure 20: Normalized ultimate fault displacement for various performance limits at different angles of β (X80 pipe, Clay I, D/t=72, pressure 46% of p_{max})